RESEARCH ARTICLE

Key Points:

- Concentrations of speciated atmospheric mercury (Hg) including gaseous elemental mercury (GEM), particulate bound mercury (PBM), and gaseous oxidized mercury (GOM) and isotopic composition of GEM were measured in the marine boundary layer (MBL) of East China Sea (ECS)
- Outflow of Hg from mainland China is the dominant source of atmospheric GEM in the MBL of ECS and drive the GEM isotopic composition toward lower δ^{202}Hg and higher Δ^{199}Hg values
- Using a binary mixing model, highly negative δ^{202}Hg (-1.79 ± 0.24‰, 1σ) and near-zero Δ^{199}Hg (0.02 ± 0.04‰, 1σ) signatures for China GEM emissions is predicted

Supporting Information:
- Figure S1

Correspondence to:
X. Fu and X. Feng,
fuxuewu@mail.gyig.ac.cn;
fengxinbin@vip.skleg.cn

![JGR logo]

![Check for updates]

Isotopic Composition of Gaseous Elemental Mercury in the Marine Boundary Layer of East China Sea

Xuewu Fu[1] (iD), **Xu Yang[2]** (iD), **Qingyou Tan[1]**, **Lili Ming[3]**, **Tian Lin[1]**, **Che-Jen Lin[1,4]**, **Xiangdong Li[3]** (iD), and **Xinbin Feng[1]** (iD)

[1]State Key Laboratory of Environmental Geochemistry, Institute of Geochemistry, Chinese Academy of Sciences, Guiyang, China, [2]Observatoire Midi-Pyrénées, Laboratoire Géosciences Environnement Toulouse, CNRS/IRD/Université de Toulouse, Toulouse, France, [3]Department of Civil and Environmental Engineering, The Hong Kong Polytechnic University, Kowloon, Hong Kong, [4]Center for Advances in Water and Air Quality, Lamar University, Beaumont, TX, USA

Abstract Characterizing the speciation and isotope signatures of atmospheric mercury (Hg) downwind of mainland China is critical to understanding the outflow of Hg emission and the contributing sources. In this study, we measured the concentrations of gaseous elemental mercury (GEM), particulate bound mercury, gaseous oxidized mercury, and the GEM isotopic composition in the marine boundary layer of East China Sea from October 2013 to January 2014. Mean ($\pm 1\sigma$) GEM, particulate bound mercury, and gaseous oxidized mercury concentrations were 2.25 ± 1.03 ng/m^3, 26 ± 38 pg/m^3, and 8 ± 10 pg/m^3, respectively. Most events of elevated GEM are associated with the outflow of Hg emissions in mainland China. The 24- and 48-hr integrated GEM samples showed large variations in both δ^{202}Hg (-1.63‰ to 0.34‰) and Δ^{199}Hg (-0.26‰ to -0.02‰). GEM δ^{202}Hg and Δ^{199}Hg were negatively and positively correlated to its atmospheric concentrations, respectively, suggesting a binary physical mixing of regional background GEM and Hg emissions in mainland China. Using a binary mixing model, highly negative δ^{202}Hg (-1.79 ± 0.24‰, 1σ) and near-zero Δ^{199}Hg (0.02 ± 0.04‰, 1σ) signatures for China GEM emissions are predicted. Such isotopic signatures are significantly different from those found in North America and Europe and the background global/regional atmospheric GEM pool. It is likely that emissions from industrial and residential coal combustion (lacking conventional air pollutant control devices), cement and mercury production, biomass burning, and soil emissions contributed significantly to the estimated isotope signatures of GEM emissions in China.

1. Introduction

Mercury (Hg) is a toxic pollutant to humans and wildlife. The levels and isotopic compositions of Hg in the Earth's surface reservoirs largely depend on the transformation and transport of Hg in the atmosphere (Blum et al., 2014; Lamborg et al., 2014). Both anthropogenic and natural sources contribute to Hg release into the atmosphere. Anthropogenic sources emit 1,900–2,300 tons of Hg annually (Pacyna et al., 2010; Pirrone et al., 2010), representing approximately one third of global total Hg emissions, whereas the remaining fraction comes from natural sources and reemission of deposited Hg (Selin et al., 2007). Atmospheric Hg occurs predominantly in the form of gaseous elemental mercury (GEM), while other forms including gaseous oxidized mercury (GOM) and particulate bound mercury (PBM) generally account for <10% of total Hg in the atmosphere (Gustin et al., 2015). Because of its mild reactivity, high volatility, and low water solubility, GEM is fairly stable with an atmospheric lifetime of several months to a year and can spread globally before deposited to the Earth's surfaces (Lindberg et al., 2007). In contrast, GOM and PBM have much higher dry deposition velocity and water solubility and can be readily removed from the atmosphere (Wright et al., 2016; Zhang et al., 2016).

Hg has seven stable isotopes with atomic mass ranging from 196 to 204 (Bergquist & Blum, 2007). Since the development of multicollector inductively coupled plasma mass spectrometry (MC-ICPMS) method and improvements of sample collection and processing, important advances have been achieved in the measurement of Hg isotopic compositions in geogenic and environmental samples (Blum et al., 2014). The reported mass-dependent Hg isotope fractionation (MDF, δ^{202}Hg signature) and mass-independent fractionation (MIF, Δ^{199}Hg, Δ^{201}Hg signatures) of odd Hg isotopes varied significantly in a range exceeding 10‰ (Blum et al., 2014; Sonke & Blum, 2013). The observed fractionation and variability have been attributed to environmental processes including reduction/oxidation, methylation/demethylation, adsorption/desorption, or evaporation (Bergquist & Blum, 2007; Estrade et al., 2009; Kritee et al., 2008; Rodriguez-Gonzalez et al., 2009; Wiederhold et al., 2009; Zheng et al., 2007; Zheng & Hintelmann, 2009). The unusual MIF of even Hg isotopes (Δ^{200}Hg,

Δ^{204}Hg signatures) has been also observed in precipitation and atmospheric GEM, PBM, and GOM (Chen et al., 2012; Demers et al., 2013; Gratz et al., 2010; Rolison et al., 2013). Although the environmental processes driving the MDF and MIF of Hg isotopes need to be further investigated, the isotopic signature serves as an important signal for tracing the sources, transformation, and cycling of Hg in the environment (Blum et al., 2014).

Recently, several studies have reported isotopic compositions of total gaseous mercury (TGM = GEM + GOM) in the planetary boundary layer (PBL) and in the free troposphere in North America and Europe (Demers et al., 2013, 2015; Enrico et al., 2016; Fu, Maruszczak, Wang, et al., 2016; Gratz et al., 2010; Obrist et al., 2017; Sherman et al., 2010). These studies found that δ^{202}Hg of TGM from anthropogenic sources is lower than the value observed in the background atmospheric Hg pool, which is characterized by moderately positive δ^{202}Hg values (Demers et al., 2015; Fu, Maruszczak, Wang, et al., 2016; Gratz et al., 2010). Processes including foliar uptake and oxidation of atmospheric GEM have been suggested to be responsible for the positive δ^{202}Hg of TGM in the global Hg background (Demers et al., 2013; Fu, Maruszczak, Wang, et al., 2016). China is the single largest source country of atmospheric Hg in the world (Pacyna et al., 2010; Pirrone et al., 2010), and therefore, its emissions play an important role in the global cycling of atmospheric Hg. As a newly industrializing country, proportion of anthropogenic Hg emissions from various source sectors in China are different from those in Europe and North America. For example, emission from coal-fired power plants (CFPPs) is the dominant anthropogenic Hg source in Europe and North America, accounting for 55–70% of the total anthropogenic Hg emissions in these regions (Muntean et al., 2014), and these values are much higher than that (18.8%) in China (Zhang et al., 2015). In China, anthropogenic Hg emissions are mainly derived from industrial and residential coal combustion, nonferrous metal smelting, and cement production, accounting for 63.3% of the total anthropogenic Hg emissions (Zhang et al., 2015). Isotopic signatures of Hg emitted anthropogenic sources could be influenced by the isotopic signatures of Hg in different source materials and air pollution control devices (APCDs; Sun, Heimburger, et al., 2013; Sun et al., 2016). Application rates of APCDs in industrial and residential coal combustion are much lower than CFPPs (Wu et al., 2016) and would therefore not induce significant positive shifts of δ^{202}Hg of emitted GEM relative to feed source materials as that of CFPPs (Sun et al., 2016). Isotopic compositions of GEM emitted from zinc smelting and cement production were estimated to have much more negative δ^{202}Hg values than that emitted from CFPPs (Sun et al., 2016; Tang et al., 2017). As a consequence, isotopic signatures of Hg emitted from Chinese anthropogenic sources would differ from those in North America and Europe. Hence, there is a need to study the isotopic compositions of atmospheric Hg in China for characterizing the isotopic compositions of Hg emissions in China and background regional atmospheric Hg pool, which in turn helps to understand the impact of Chinese emission on regional/global atmospheric Hg budget.

Dynamics of atmospheric Hg in the marine boundary layer (MBL) is of interest because of the large fraction of GEM emitted from the ocean and the enhanced atmospheric GEM oxidation (Laurier et al., 2003; Mao et al., 2016; Strode et al., 2007; Wang et al., 2014). A pervious TGM isotope study in the Grand Bay, Mississippi, USA, showed highly negative δ^{202}Hg (<2‰) in oceanic air masses, reflecting photoreduction, and evasion of Hg from the ocean (Rolison et al., 2013). Recent studies in the coastal Pensacola, Florida, USA, and the Pic du Midi Observatory, France, however, suggest that oceanic air mass is characterized by moderate positive TGM δ^{202}Hg (means of 0.77‰ and 0.43‰, respectively; Demers et al., 2015; Fu, Maruszczak, Wang, et al., 2016), which were likely a result of atmospheric oxidation that increases GEM δ^{202}Hg in the heavier isotopes (Fu, Maruszczak, Wang, et al., 2016).

In the present study, concentrations and isotopic composition of atmospheric GEM were measured at Huaniao Island (HNI) in the MBL of East China Sea (ECS). To the best of our knowledge, this is the first study to directly measure GEM isotopic composition in the MBL. HNI regularly receives Hg-polluted air masses originated from the PBL of mainland China and clean air masses from the West Pacific Ocean (Figure S1). The observations provide an insight into the isotopic signatures of Hg sources in mainland China and the background atmospheric Hg pool in East Asia as well as the sources of atmospheric Hg in the MBL of ECS.

2. Materials and Methods

2.1. Site Description

HNI (30.86°N, 122.67°E) is a small island (3.2 km^2) located in the ECS and approximately 66 km east of shore of Shanghai (Figure S1). The sampling site was located on the north edge of HNI and approximately 50 m from

the ocean. There were no industrial activities and fossil fuel consumption at HNI. The population in HNI is ~800 and mostly concentrated in the southwest of HNI, which plays a minor role in the observations under the dominant northwestern monsoonal wind during the study period.

2.2. Atmospheric Hg Speciation Measurements

Atmospheric GEM, PBM, and GOM at 5 m above ground level were continuously measured using the Tekran® 2537/1130/1135 system (Tekran Inc., Canada) from 22 October 2013 to 6 January 2014 (Malcolm et al., 2003). Atmospheric GOM and PBM were collected onto KCl-coated annular denuder and quartz fiber filter in sequence at 1-hr intervals at a volumetric flow rate of 10 L/min (LPM). During the collection of GOM and PBM, GEM was trapped by dual gold cartridges at 5-min interval at a mass flow rate of 1.0 LPM and subsequently thermally decomposed and detected by the cold vapor atomic fluorescence spectroscopy (CVAFS). Once collected, GOM and PBM are thermally decomposed from each unit and detected by CVAFS as Hg^0. KCl-coated denuder, Teflon coated glass inlet, and impactor plate were replaced every 10 days, and quartz filters were replaced every 20 days. Denuders and quartz filters were prepared and cleaned before field sampling following the methods in Tekran technical notes. The Tekran® 2537 analyzer was routinely calibrated using its internal permeation source at a 47-hr interval.

2.3. Backward Trajectory and Potential Source Identification at HNI

The potential source regions of elevated atmospheric GEM ($>$1.5 ng/m^3) observed at HNI are identified using a Potential Source Contribution Function (PSCF) approach (Fu, Maruszczak, Heimburger, et al., 2016), based on the every 2-hr calculations of seven-day backward trajectories ending at HNI using the TrajStat Geographical Information System based software (Wang et al., 2009). The criterion of the elevated GEM ($>$1.5 ng/m^3) is when the concentration is greater than the background GEM concentrations in the Northern Hemisphere (Sprovieri et al., 2016). We also identified the potential source regions of low atmospheric GEM ($<$1.5 ng/m^3) at HNI using the PSCF approach. To differentiate from the potential source regions associated with elevated atmospheric GEM (indicated by the PSCF values), the potential source regions of low atmospheric GEM are indicated by Potential Background Contribution Function (PBCF) values. Fractional atmospheric air masses residence time (ARTs, i.e., the percent of time an air mass spent over different regions) over mainland China, other continents in Asia (including Russia), and oceans (mostly of the ECS, Yellow Sea, and West Pacific Ocean) were estimated from seven-day backward trajectories. The three-dimensional locations of air masses predicted by backward trajectory have an uncertainty of up to 40% for seven-day trajectories (Engstrom & Magnusson, 2009). However, given the large number of trajectory endpoints utilized in PSCF and PBCF modeling, the uncertainty of the locations of identified source region is substantially reduced. Besides, the "trailing effect," selection of concentration threshold, transformation, and deposition of atmospheric Hg during transport can affect the PSCF and PBCF receptor model (Cheng et al., 2015), which were not evaluated in the present study. Therefore, the identified source regions of elevated and low atmospheric GEM should be regarded as potential source contributors only.

2.4. GEM Collections and Processing for Isotope Analysis

TGM at HNI was collected on chlorine-impregnated activated carbon (CLC, 1.0 g) traps at volumetric flow rates of 10–12 LPM. Detailed information regarding the preparation of CLC can be found in Fu et al. (2014). Atmospheric TGM consists of GEM and GOM. Under the sampling conditions (24 and 48 hr) in this study, GOM generally made up a small portion of TGM (on average 0.35% of TGM and never exceeds 1.3%). Recent studies suggested that GOM concentrations measured by KCl-coated denuders can be underestimated by a factor of 2 to 3 (Gustin et al., 2015). The average fraction of GOM in TGM could therefore increase up 1.0% and temporarily up to 3.9%. Therefore, the minor fraction of GOM in TGM at HNI is unlikely to bias the measured TGM isotopic composition, which is equivalent to the GEM isotopic compositions. Blanks of the CLC traps were determined with values $<$0.4 ng ($n = 8$), negligible compared to the amount of GEM collected during field sampling (10–55.3 ng Hg per sample). GEM collection recoveries of the CLC traps at flow rates of 10–12 LPM were determined by measuring the breakthrough of GEM during a sampling period of 24 hr (i.e., we used a CLC trap that consists of two sections within the same trap to estimate the GEM sampling efficiency. The second section (downstream of the first section which contains 1.0 g of CLC) containing of 0.2 g of CLC was used to measure breakthrough concentrations. The collection

efficiency can be defined as GEM concentrations measured by the first section relative to the sum of first and second sections. The collection recoveries of the CLC traps were in the range of 97.4–99.8% (mean [±1σ] = 98.4 ± 1.0% [$n = 6$]). Atmospheric particles were removed using a 47-mm diameter Teflon filter (pore size 0.2 μm) installed at the inlet of CLC traps. CLC traps were kept warm (50–70 °C) during sampling to avoid water condensation. Sampling of GEM isotopes was conducted from 21 October to 25 November 2014 and from 13 to 23 December 2014 with sampling durations of 24 and 48 hr, respectively. After the field sampling, CLC traps were sealed carefully and kept in a clean environment until preconcentration into trap solutions for Hg isotope analysis.

GEM collected on CLC traps was preconcentrated into 5–10 ml of 40% mixed acid solution (v/v, $2HNO_3$/$1HCl$) using a double-stage combustion protocol described before for Hg isotope analysis (Biswas et al., 2008; Sun, Enrico, et al., 2013). Briefly, GEM in CLC traps was thermally released through combustion using a Hg-free oxygen flow (25 ml/min), and then the combustion products were further decomposed in a hot quartz tube (1000 °C). The combustion released all the Hg in the form of Hg^0, which was subsequently sparged into mixed acid solution. After the completion of the combustion, the trapping bottles and impingers were rinsed 3 times with Milli-Q water. The rinsed water was added to trapping solutions to yield an acid concentration of ~20% for Hg isotope analysis. The final trapping solutions were kept in a refrigerator at 2–4 °C until the isotope analysis. Full procedural blanks of the combustion system and CLC traps were investigated by combustion of 1.0 g of CLC and showed a mean (±1σ) of 0.034 ± 0.007 ng/ml ($n = 4$), which accounted for a mean (±1σ) of 2.2 ± 0.8% of Hg concentrations in filed sample trapping solutions. The recoveries of preconcentration of CLC traps were tested by combusting standard reference material BCR 482 (lichen, 480 ng/g) using the same combustion protocol of CLC traps. Mean (±1σ) recoveries of the combustion was 94.3 ± 3.6% ($n = 4$).

2.5. Mercury Isotope Analysis

Hg isotope ratios were measured using cold vapor MC-ICPMS (Thermo-Finnigan Neptune) at the State Key Laboratory of Ore Deposit Geochemistry, CAS, Guiyang, China, following the method described in a previous study (Yin et al., 2010). Instrumental mass bias of MC-ICPMS was corrected by standard-sample-standard bracketing using NIST 3133 Hg at matching concentrations. Hg isotopic composition is reported in delta notation (δ) in per mil referenced to the bracketed NIST 3133 Hg standard (Blum & Bergquist, 2007):

$$\delta^{xxx}Hg = \left(\frac{\left(^{xxx}Hg^{198}Hg\right)_{sample}}{\left(^{xxx}Hg^{198}Hg\right)_{SRM3133}} - 1 \right) \times 1000‰ \tag{1}$$

MIF values are expressed by "capital delta (Δ)" notation (‰), which is the difference between the measured values of $\delta^{199}Hg$, $\delta^{200}Hg$, $\delta^{201}Hg$, and those predicted from $\delta^{202}Hg$ using the kinetic MDF law (Blum & Bergquist, 2007):

$$\Delta^{199}Hg\ (‰) = \delta^{199}Hg - \left(0.252 \times \delta^{202}Hg\right) \tag{2}$$

$$\Delta^{200}Hg\ (‰) = \delta^{200}Hg - \left(0.502 \times \delta^{202}Hg\right) \tag{3}$$

$$\Delta^{201}Hg\ (‰) = \delta^{201}Hg - \left(0.752 \times \delta^{202}Hg\right) \tag{4}$$

The analytical uncertainty of isotopic analysis was obtained by repeated analysis of the UM-Almaden standard over different analysis. The overall mean (±2σ) values of $\delta^{202}Hg$, $\Delta^{199}Hg$, $\Delta^{200}Hg$, and $\Delta^{201}Hg$ for all the UM-Almaden standards were −0.54 ± 0.08‰, −0.01 ± 0.06‰, 0.01 ± 0.06‰, and −0.01 ± 0.08‰ ($n = 15$), respectively, in excellent agreement with previously reported values (Blum & Bergquist, 2007). Mean (±2σ) values of $\delta^{202}Hg$, $\Delta^{199}Hg$, $\Delta^{200}Hg$, and $\Delta^{201}Hg$ for the standard reference material BCR 482 were −1.65 ± 0.17‰, −0.61 ± 0.06‰, 0.07 ± 0.03‰, and −0.64 ± 0.10‰ ($n = 4$), which were comparable with literature data (Estrade et al., 2010). The analytical uncertainty of isotopic composition of GEM samples in this study is represented as the larger 2σ values from either the analytical replicates or the measurements of UM-Almaden standards.

3. Results and Discussion

3.1. Hg Speciation and Sources

Mean (±1σ) atmospheric GEM, PBM, and GOM concentrations at HNI during the study period were 2.25 ± 1.03 ng/m^3, 26 ± 38 pg/m^3, and 8 ± 10 pg/m^3, respectively. Atmospheric Hg varied significantly with the maximum GEM (5-min mean), PBM (hourly mean), and GOM (hourly mean) concentrations of 13.9 ng/m^3, 422 pg/m^3, and 97 pg/m^3, respectively (Figure S2). The mean GEM, PBM, and GOM levels at HNI were consistent with observations in remote areas of China (Fu et al., 2015) but relatively higher than those observed in MBL in the North Pacific Ocean, Mediterranean Sea, East Pacific Ocean, Subtropical Atlantic Ocean, and South Indian Ocean (GEM = 0.85 to 2.04 ng/m^3, PBM = 1 to 3 pg/m^3, and GOM = 2 to 8 pg/m^3; Chand et al., 2008; Laurier & Mason, 2007; Mao et al., 2016; Slemr et al., 2015; Sprovieri et al., 2003; Wang et al., 2014).

Our measurements reveal that outflow of Hg from mainland China was the major source of atmospheric GEM at HNI (Figure 1). The major source regions of elevated atmospheric GEM at HNI were dominantly from the PBL over eastern and central China, including Shanghai metropolitan area, Jiangsu, Zhejiang, Anhui, Shandong, Henan, Hubei, and Jiangxi provinces (Figures 1 and S3). The total anthropogenic Hg emissions in these regions were estimated to be 208 tons in 2010, accounting for 39.3% of the total anthropogenic Hg emissions in China (Zhang et al., 2015). On the other hand, low atmospheric GEM at HNI was mostly associated with air mass from the open seas of ECS, the Yellow Sea, and the free troposphere over Northeast Asia (Figures 1 and S3).

3.2. GEM Isotopic Compositions

Isotopic compositions of atmospheric GEM at HNI (n = 34) varied from −1.63‰ to 0.34‰ (mean [±1σ] = −0.21 ± 0.39‰) for δ^{202}Hg, −0.26‰ to −0.02‰ (mean [±1σ] = −0.16 ± 0.06‰) for Δ^{199}Hg, −0.11‰ to 0.03‰ (mean [±1σ] = −0.06 ± 0.03‰) for Δ^{200}Hg, and −0.32‰ to 0.08‰ (mean [±1σ] = −0.18 ± 0.08‰) for Δ^{201}Hg (Figure 2 and Table S1). A comparison of the isotopic compositions of atmospheric TGM/GEM between this and previous studies is shown in Table S2 in the supporting information (Demers et al., 2013, 2015; Enrico et al., 2016; Fu, Maruszczak, Wang, et al., 2016; Fu, Zhu, et al., 2016; Gratz et al., 2010; Obrist et al., 2017; Rolison et al., 2013; Sherman et al., 2010; Xu et al., 2017; Yu et al., 2016). The δ^{202}Hg values of GEM at HNI were much lower than those measured in the free troposphere of Pic du Midi Observatory (mean [±1σ] = 0.17 ± 0.14‰) and forested Pinet peat bog (mean [±1σ] = 1.19 ± 0.13‰) in France and those in the Great Lakes region (mean [±1σ] = 0.21 ± 0.30‰), Wisconsin forest (mean [±1σ] = 0.75 ± 0.24‰), coastal region of Pensacola, Florida (mean [±1σ] = 0.84 ± 0.25‰), and Alaska (mean [±1σ] = 0.67 ± 0.09‰) in the United States (Demers et al., 2013, 2015; Enrico et al., 2016; Fu, Maruszczak, Wang, et al., 2016; Gratz et al., 2010; Obrist et al., 2017) but higher than or comparable to those measured in urban Beijing (mean [±1σ] = −0.73 ± 0.57‰), Guiyang (mean [±1σ] = −0.56 ± 0.21‰), and Xi'an (mean [±1σ] = −0.08 ± 0.41‰), China (Xu et al., 2017; Yu et al., 2016). The Δ^{199}Hg values of GEM at HNI were comparable to the observations at remote sites in the United States (e.g., the Great Lake region, mean [±1σ] = −0.12 ± 0.06‰; Wisconsin forest, mean [±1σ] = −0.19 ± 0.03‰; coastal region of Pensacola, Florida, mean [±1σ] = −0.23 ± 0.05‰; and Alaska, mean [±1σ] = −0.25 ± 0.04‰) and France (e.g., the Pic du Midi Observatory, mean [±1σ] = −0.21 ± 0.03‰, and forested Pinet peat bog, mean [±1σ] = −0.17 ± 0.07‰; Demers et al., 2013, 2015; Enrico et al., 2016; Fu, Maruszczak, Wang, et al., 2016; Gratz et al., 2010; Obrist et al., 2017) but slightly lower than those measured in urban Beijing (mean [±1σ] = −0.03 ± 0.07‰), Guiyang (mean [±1σ] = 0.04 ± 0.05‰), and Xi'an (mean [±1σ] = 0 ± 0.04‰), China (Xu et al., 2017; Yu et al., 2016).

Global observations indicate significant variations in δ^{202}Hg (−2.03 to 1.43‰) and Δ^{199}Hg (−0.31 to 0.15‰). Regional mean GEM δ^{202}Hg rank in a descending order at U.S. remote sites, European remote sites, MBL of ECS, and then Chinese urban sites, whereas global spatial variations of GEM Δ^{199}Hg are in a reverse order with more negative Δ^{199}Hg observed in the United States and at remote European sites, and Δ^{199}Hg near zero in Chinese urban areas (Figure 2). These variations can be attributed to a number of reasons including the different proportions of background global atmospheric Hg pool and regional emissions contributing to the atmospheric GEM budget, in situ atmospheric Hg transformations, and the specific isotopic signatures of Hg emissions from different regions. Due to the large domestic anthropogenic Hg emissions, modeling studies estimated that local anthropogenic sources contributed at least 30% to the surface GEM concentrations in mainland China, and this value is higher than that in the nearshore zone and open seas of ECS (10–30%),
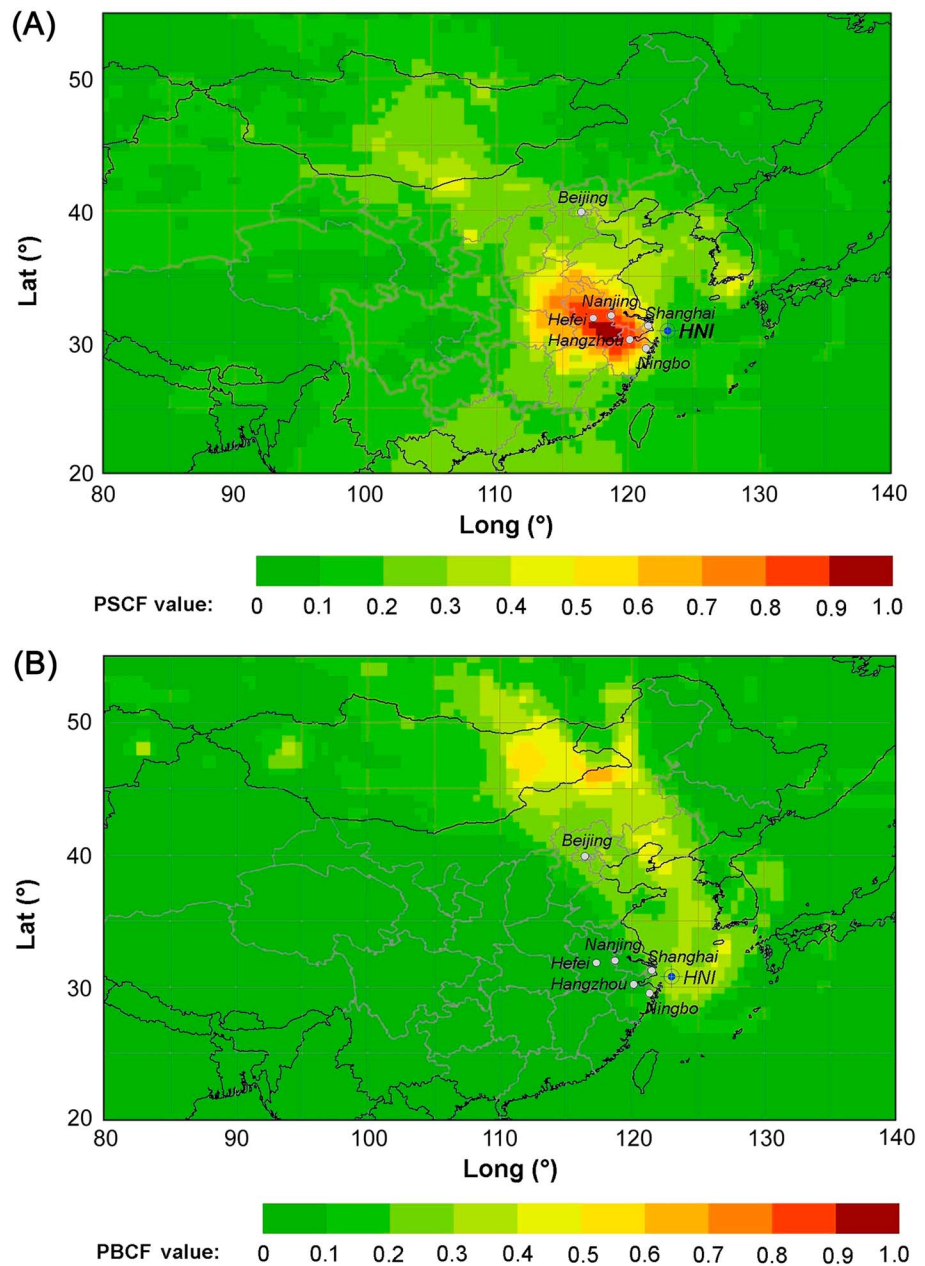
Figure 1. Potential source regions associated with (a) elevated atmospheric GEM concentrations (>1.5 ng/m^3) and (b) low atmospheric GEM concentration (<1.5 ng/m^3) at HNI, ECS.

Europe (11.3%), and North America (5.5%; Chen et al., 2015, 2014). GEM originated from global anthropogenic sources has moderately negative δ^{202}Hg (mean = −0.59‰) and Δ^{199}Hg close to zero (mean = −0.02‰; Sun et al., 2016), which are significantly lower and higher than the δ^{202}Hg (mean [±1σ] = 0.84 ± 0.22‰) and Δ^{199}Hg (mean [±1σ] = −0.21 ± 0.04‰) of atmospheric GEM observed in remote areas not affected by direct anthropogenic emissions (e.g., Wisconsin forest, coastal region of Pensacola impacted by oceanic and free tropospheric air, and Alaska in the United States and forested Pinet peat bog in France), respectively (Demers et al., 2013, 2015; Enrico et al., 2016; Obrist et al., 2017). Therefore, the large proportions of local anthropogenic emissions in atmospheric GEM budget in mainland China and MBL of ECS drive the GEM isotopic compositions toward lower δ^{202}Hg and higher Δ^{199}Hg values. GEM isotopic compositions could also be modified by natural environmental processes. Atmospheric GEM in forests worldwide generally had positive δ^{202}Hg values mainly due to the preferential uptake of lighter
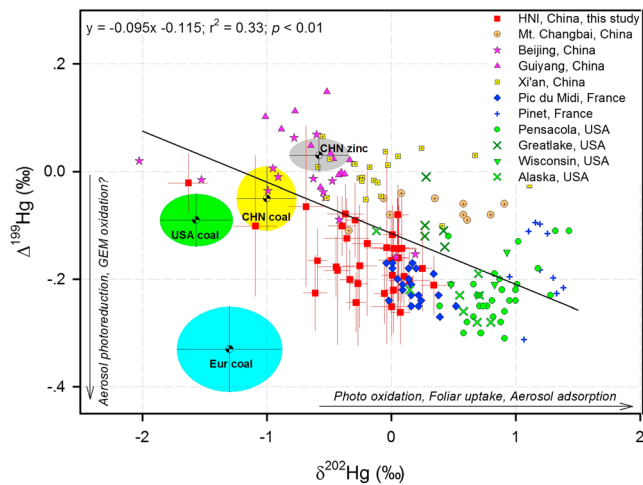
Figure 2. Mass-dependent (δ^{202}Hg) and mass-independent (Δ^{199}Hg) isotope signatures of atmospheric TGM/GEM and source materials (e.g., China, United States, and European feed coal and China zinc ores) worldwide. The error bar on δ^{202}Hg and Δ^{199}Hg of atmospheric GEM at HNI and source materials indicates 2σ and 1σ of isotopic measurement, respectively. The black line represents the relationship between GEM δ^{202}Hg and Δ^{199}Hg for the global observations. Data are from this study and the literature (Demers et al., 2013, 2015; Enrico et al., 2016; Fu, Maruszczak, Wang, et al., 2016; Fu, Zhu, et al., 2016; Gratz et al., 2010; Lefticariu et al., 2011; Obrist et al., 2017; Sun et al., 2014; Yin et al., 2014, 2016; Yu et al., 2016).

isotopes by foliage (Demers et al., 2013; Enrico et al., 2016; Fu, Zhu, et al., 2016). Oceanic emission and oxidation of atmospheric GEM are the two important processes influencing the atmospheric GEM dynamics in MBL. Modeled contribution of oceanic emission to atmospheric GEM concentrations in the MBL of ECS is ranging from 20 to 40% (Soerensen et al., 2010). The isotopic composition of GEM emitted from ocean is poorly constrained. However, previous studies analyzed the air masses from ocean and suggested that GEM in MBL was characterized by moderately positive δ^{202}Hg values (Demers et al., 2015; Fu, Maruszczak, Wang, et al., 2016). Hence, mixing of clean oceanic air masses would probably result in higher δ^{202}Hg$_{GEM}$ at HNI compared to Chinese urban areas. It should also be noted that two GEM samples at HNI were observed with δ^{202}Hg values (−1.09‰ and −1.63‰) significantly lower than the average δ^{202}Hg (−0.59‰) of global anthropogenic emission sources. These samples were mainly impacted by outflow of Hg from mainland China and indicated that Hg emissions from mainland China may have much lower δ^{202}Hg values relative to the mean of global anthropogenic emission sources, which is further discussed in the following sections.

3.3. Relationship Between Concentrations of Atmospheric Hg and GEM Isotopic Composition

The δ^{202}Hg of GEM was negatively correlated with GEM concentrations, while the Δ^{199}Hg$_{GEM}$ showed positive correlation with GEM concentrations at HNI during the study period (Figure 3). The correlations suggest a binary mixing of end-member sources, with one end-member characterized as elevated GEM concentrations, highly negative GEM δ^{202}Hg, and near-zero GEM Δ^{199}Hg values and the other end-member characterized as low GEM concentrations, moderately positive GEM δ^{202}Hg, and negative GEM Δ^{199}Hg values. A recent GEM isotope study at the Pic du Midi Observatory, France, observed higher GEM δ^{202}Hg for free tropospheric Atlantic Ocean air masses with elevated GOM concentrations but not for the Atlantic MBL air masses (Fu, Maruszczak, Wang, et al., 2016). In this study, no significant relationship was found between atmospheric GOM concentrations and Δ^{199}Hg$_{GEM}$ or δ^{202}Hg$_{GEM}$ (Figure S4; p values for both >0.05). This suggests that

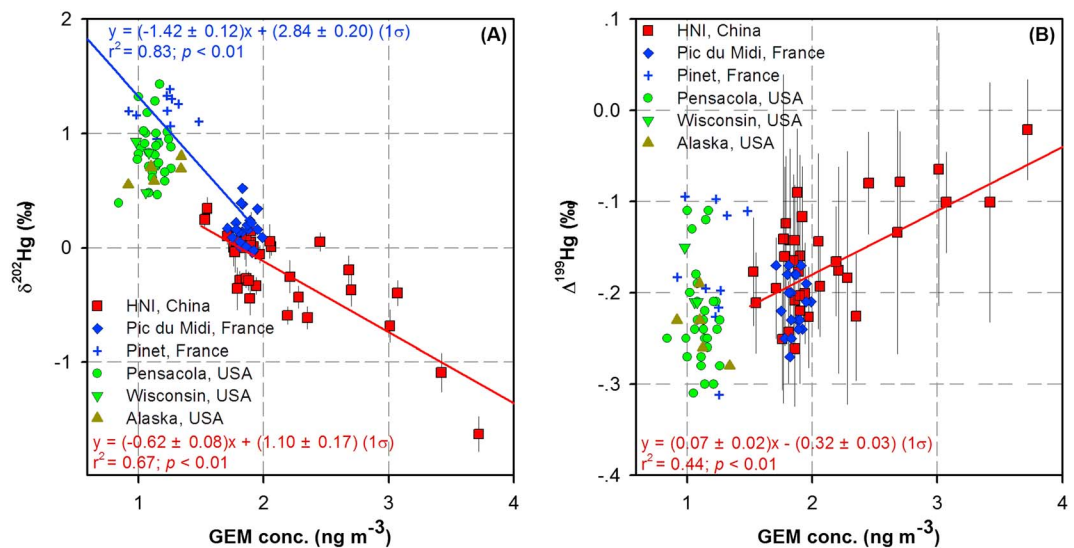**Figure 3.** Relationship between atmospheric GEM concentrations and (a) GEM δ^{202}Hg and (b) GEM Δ^{199}Hg (error bars on GEM δ^{202}Hg and Δ^{199}Hg indicates 2σ uncertainty) in this study, Europe, North America, and Arctic. Data are from this study and the literature (Demers et al., 2013, 2015; Enrico et al., 2016; Fu, Maruszczak, Wang, et al., 2016; Obrist et al., 2017).

mixing of sources and/or air masses rather than atmospheric GEM oxidation was the main cause for the variation of GEM isotopic compositions in the MBL of ECS.

During the campaign at HNI, air masses mainly originated from mainland China (mean fractional ARTs = 25%), other Asian regions (mean fractional ARTs = 41%), and oceans (e.g., ECS, Yellow Sea, and West Pacific Ocean, mean fractional ARTs = 34%). Identified potential source regions suggested that elevated GEM concentrations at HNI were mostly associated with the outflow from mainland China (Figure 1). In addition, the GEM δ^{202}Hg values were significantly negatively correlated with fractional Chinese ARTs ($r^2 = 0.31$, $p < 0.01$) and no significant relationship existed between GEM Δ^{199}Hg values and fractional Chinese ARTs ($r^2 = 0.05$, $p = 0.21$; Figure S5). Due to the impacts of domestic emissions, previous studies in urban China observed highly elevated GEM concentrations (mean [$\pm 1\sigma$] = 9.20 ± 7.56 ng/m^3), negative GEM δ^{202}Hg (mean [$\pm 1\sigma$] = −0.40 ± 0.51‰), and near-zero GEM Δ^{199}Hg (mean [$\pm 1\sigma$] = 0.00 ± 0.06‰; Fu et al., 2015; Xu et al., 2017; Yu et al., 2016). These findings suggest that Chinese emissions represented an end-member source at HNI (hereafter, referred to as Chinese sources, characterized by elevated GEM concentration, highly negative GEM δ^{202}Hg, and near-zero GEM Δ^{199}Hg). In contrast, low GEM concentrations at HNI were mainly associated with air masses from open seas of ECS and Yellow Sea and the Asian free troposphere (Figure 1). This is consistent with previous modeling results that atmospheric GEM concentrations in these regions ranged from 1.2 to 1.6 ng/m^3 (Lin et al., 2010; Pan et al., 2010). Based on the correlations between GEM concentrations and GEM isotopic compositions observed in this study, it is likely that open seas and the Asian free troposphere represented the other end-member source at HNI (hereafter, referred to as regional background, characterized by low GEM concentration, moderately positive δ^{202}Hg$_{GEM}$, and negative Δ^{199}Hg$_{GEM}$). These regions receive little (e.g., <20%) influence from anthropogenic emissions and therefore represent regional background atmospheric pool (Pan et al., 2010). Clear difference in GEM isotope MDF (δ^{202}Hg) signatures between emission sources and regional background atmospheric pool has been observed in Europe and North America (Demers et al., 2015; Fu, Maruszczak, Wang, et al., 2016; Gratz et al., 2010). To our knowledge, this is the first study identifying that distinguishable MDF (δ^{202}Hg) and MIF (Δ^{199}Hg) signatures of GEM exist between emission sources in mainland China and the background atmospheric pool in East Asia.

Similar relationships between GEM concentrations and GEM δ^{202}Hg were also observed in North America and Europe (Figure 3). Observations in North America and Europe generally showed lower GEM concentrations (0.84 to 1.99 ng/m^3), positive GEM δ^{202}Hg, and moderately negative Δ^{199}Hg (Demers et al., 2013, 2015; Enrico et al., 2016; Fu, Maruszczak, Wang, et al., 2016; Obrist et al., 2017), while observations in this study showed higher GEM concentrations (1.53 to 3.72 ng/m^3), lower GEM δ^{202}Hg, and higher Δ^{199}Hg values. The correlation slopes of δ^{202}Hg/GEM$_{conc.}$ (−0.61 ± 0.08‰/(ng/m^3)) and Δ^{199}Hg/GEM$_{conc.}$ (0.07 ± 0.02‰/ng/m^3) in ECS differ from those in Europe (δ^{202}Hg/GEM$_{conc.}$ correlation slope = −1.42 ± 0.12‰/ng/m^3; and no significant relationship existed between GEM Δ^{199}Hg and concentrations) and North America (no significant relationship existed between GEM δ^{202}Hg, Δ^{199}Hg, and GEM concentrations; Figure 3). It should be noted that 70% of the GEM samples in North America and Europe had concentrations lower than the background values (1.53 ng/m^3) in the Northern Hemisphere (Sprovieri et al., 2016), whereas all the GEM samples at HNI had concentrations higher than the background in the North Hemisphere (Figure 3). The sampling sites in North America and Europe were mostly located in the vegetation-covered regions (e.g., forest and tundra) and/or free troposphere. In these regions, atmospheric transformations including foliar uptake and atmospheric oxidation could deplete GEM concentration quickly (Fu, Zhu, et al., 2016; Swartzendruber et al., 2006), and consequently resulted in GEM concentrations lower than the background in the North Hemisphere. At the same time, foliar uptake and atmospheric oxidation of GEM could shift the GEM isotopic compositions toward higher δ^{202}Hg values (Demers et al., 2013; Enrico et al., 2016; Fu, Maruszczak, Wang, et al., 2016). Therefore, atmospheric transformations should play a more important role in regulating the correlation slopes of δ^{202}Hg/GEM$_{conc.}$ in Europe and North America than mixing of sources. This is different from HNI where mixing of sources played a more important role.

3.4. Probing Isotopic Composition of GEM Emissions in China and Regional Background Atmospheric GEM Pool

The isotopic compositions of GEM emissions in mainland China and regional background atmospheric GEM pool (e.g., the open seas and free troposphere in East Asia) end-members are estimated using the linearized δ^{202}Hg versus 1/GEM$_{conc.}$ and Δ^{199}Hg versus 1/GEM$_{conc.}$ physical mixing diagrams (Figure 4; Xu et al., 2017).

Figure 4. (a) δ^{202}Hg versus 1/GEM and (b) Δ^{199}Hg versus 1/GEM diagrams suggesting a binary mixing of regional background atmospheric GEM pool and Chinese (CHN) emissions of GEM.

Extrapolating 1/GEM$_{conc.}$ to 0 (i.e., the air mass contains a negligible fraction of background atmospheric GEM) yields a δ^{202}Hg value of -1.79 ± 0.24‰ (1σ) and a Δ^{199}Hg value of 0.02 ± 0.04‰ (1σ) for the GEM emissions in mainland China. The δ^{202}Hg of GEM emissions in mainland China was more negative than the estimated mean value (-0.59‰) of global anthropogenic emissions and that (-0.44‰) estimated for local anthropogenic GEM emissions in urban Xi'an in northwestern China (Sun et al., 2016; Xu et al., 2017). The Δ^{199}Hg of GEM emissions in mainland China was comparable to the estimated mean value (-0.02‰) of global anthropogenic emissions (Sun et al., 2016). The difference in estimated δ^{202}Hg signatures between this and previous studies could be partly attributed to the regional variations in proportion of Hg emissions from various emission sectors. Sun et al. (2016) compiled Hg isotopic compositions of global source materials and suggested a large difference in δ^{202}Hg and a small difference in Δ^{199}Hg among various emission sectors. For example, due to the MDF of Hg isotopes during coal combustion in CFPPs, δ^{202}Hg value of GEM emitted from CFPPs (0.54 ± 0.25‰, 1σ) was much higher than those of other emission sectors such as zinc smelting (-0.76 ± 1.25‰, 1σ) and cement production (-1.64 ± 0.61‰, 1σ; Sun et al., 2016; Tang et al., 2017). The proportions of CFPPs Hg emissions in total anthropogenic Hg emissions in the world (29.1%) and urban Xi'an, northwestern China (72%), were much higher than the overall mean (18.8%) in China (Muntean et al., 2014; Xu et al., 2017; Zhang et al., 2015), which probably increased δ^{202}Hg of anthropogenic emissions in the heavier isotopes. It should be noted that the estimated isotopic compositions of GEM emissions in mainland China could be a result of a mixing of various sources (anthropogenic and natural sources) and atmospheric transformation-induced fractionation of Hg isotopes in the plume of Chinese outflow. In the following, we will therefore consider these factors to interpret the estimated δ^{202}Hg and Δ^{199}Hg signatures of anthropogenic emissions in China.

GEM in the atmosphere can be derived from anthropogenic and natural sources. A comparison of δ^{202}Hg and Δ^{199}Hg in major source materials between China and the rest of the world is shown in Figure S6 and Table S3 in the supporting information (Biswas et al., 2008; Demers et al., 2013; Lefticariu et al., 2011; Smith et al., 2008; Sonke et al., 2010; Sun et al., 2014, 2016; Thibodeau et al., 2016; Yin et al., 2014, 2016, 2013; Yu et al., 2016; Zheng et al., 2016). Mean (±1σ) Δ^{199}Hg in feed coal, zinc ores, limestone, Hg ores, and biomass in China are -0.03 ± 0.16‰, 0.02 ± 0.06‰, -0.01 ± 0.07‰, 0.01 ± 0.02‰, and -0.19 ± 0.10‰, respectively, significantly higher than those (-0.16 ± 0.18‰, -0.04 ± 0.06‰, -0.03 ± 0.08‰, -0.04 ± 0.07‰, and -0.28 ± 0.09‰, respectively) in the rest of the world (paired t test, $p < 0.05$, $T = 3.7$, $n = 5$). Assuming that isotopic signatures of GEM emissions from major anthropogenic sources resemble the MIF signatures of source materials (Sun, Heimburger, et al., 2013; Sun et al., 2014, 2016; Tang et al., 2017), Δ^{199}Hg of atmospheric GEM in mainland China, influenced by the regional anthropogenic sources, should be higher than the GEM Δ^{199}Hg in other regions worldwide, as shown in Figure 2. Coal combustion in CFPPs and nonferrous metal smelting are the two important sources of atmospheric GEM in China and other regions worldwide (Pirrone et al., 2010; Zhang et al., 2015). The mean (±1σ) δ^{202}Hg values of Chinese coal and zinc ores are -1.07 ± 0.71‰ and -0.47 ± 0.47‰, respectively, less

negative than those (mean $[\pm 1\sigma]_{\text{feed coal}} = -1.42 \pm 9‰$, mean $[\pm 1\sigma]_{\text{zinc ores}} = -0.76 \pm 0.62‰$) found in the rest of the world (Biswas et al., 2008; Lefticariu et al., 2011; Sonke et al., 2010; Sun et al., 2014; Yin et al., 2014, 2016). Assuming that the MDF of Hg isotopes during coal combustion in CFPPs (sufficiently equipped with APCDs) is more or less similar across the world; and that GEM emission from zinc smelting resembles the Hg isotope composition of zinc ore (Sun et al., 2016), GEM emission from CFPPs and zinc smelting in China would therefore have relatively higher δ^{202}Hg relative to other regions worldwide. Our study suggests an opposite pattern with lower GEM δ^{202}Hg of GEM emissions in China (Figure 4).

This discrepancy is possibly caused by other anthropogenic Hg sources. Implementation of APCDs (i.e., selective catalytic reduction, electrostatic precipitators, and wet flue gas desulfurization) during coal combustion is the major factor inducing significant Hg isotope MDF during coal combustion (Sun, Heimburger, et al., 2013; Tang et al., 2017). In China, the implementation level of selective catalytic reductions, electrostatic precipitators, and/or wet flue gas desulfurization in CFPPs is 100%, while the level in coal combustion in industrial boiler and domestic heating is <12% (Wu et al., 2016). Therefore, GEM emitted from industrial boilers and domestic heating in China should have much lower δ^{202}Hg compared to that ($0.54 \pm 0.25‰$, 1σ) of CFPPs sufficiently equipped by APCDs (Tang et al., 2017). In addition, mean ($\pm 1\sigma$) δ^{202}Hg of Hg in limestone, Hg ores, and biomass in China are $-1.40 \pm 0.51‰$, $-0.79 \pm 0.14‰$, and $-2.97 \pm 0.54‰$, respectively, lower than those ($-0.55 \pm 0.58‰$, $-0.59 \pm 0.81‰$, and $-2.22 \pm 0.22‰$, respectively) found in other regions worldwide (Demers et al., 2013; Smith et al., 2008; Sonke et al., 2010; Sun et al., 2016; Thibodeau et al., 2016; Yin et al., 2013; Yu et al., 2016; Zheng et al., 2016). GEM emitted from cement production preserves the Hg isotope composition of limestone and δ^{202}Hg of GEM emitted from Hg production is approximately shifted by $-1.12‰$ relative to Hg ores (Sun et al., 2016). Biomass burning on average releases 95.6% of Hg to the atmosphere primarily (>95%) in the form of GEM (Friedli et al., 2001) and is expected to induce little Hg isotope fractionation, and therefore, the δ^{202}Hg of GEM emitted should be nearly the same as that in biomass. These sources account for ~62% of the total anthropogenic GEM emissions in China (Zhang et al., 2015), sufficiently significant to cause a negative shift in domestic GEM δ^{202}Hg. Taking into account the proportions of GEM emission of the specific source sectors in total anthropogenic emissions in China and their δ^{202}Hg and Δ^{199}Hg signatures in Table S4 in the supporting information (Fu et al., 2017; Sun et al., 2016; Tang et al., 2017; Wang et al., 2016; Yin et al., 2015, 2013, 2016; Yu et al., 2016; Zhang et al., 2015), we estimate that the mean ($\pm 1\sigma$) δ^{202}Hg and Δ^{199}Hg for anthropogenic GEM emissions in China are $-0.82 \pm 0.63‰$ and $-0.04 \pm 0.13\%$ (Table S4), respectively. The estimated δ^{202}Hg of GEM emissions in China is comparatively lower than the mean value ($-0.59‰$) of global anthropogenic sources predicted by Sun et al (Sun et al., 2016) but comparatively higher than that ($-1.79 \pm 0.24‰$, 1σ) estimated using the mixing diagram. The more negative δ^{202}Hg signature estimated using the mixing diagram could be partly attributed to in-plume reduction of GOM emitted from anthropogenic sources. Recent studies suggested that 0–55% of emitted GOM by CFPPs was reduced to GEM in plume (Landis et al., 2014). GOM emitted by anthropogenic sources were estimated to have negative δ^{202}Hg values of $-0.77‰$ (Sun et al., 2016), and reductions of GOM might further shift the isotopic composition of GEM product toward more negative δ^{202}Hg values (Bergquist & Blum, 2007; Zheng & Hintelmann, 2009). In addition, soil GEM emission is another factor for the highly negative GEM δ^{202}Hg observed in China. Soil GEM emissions are much higher in China than that in the rest of the world (Wang et al., 2016; Zhu et al., 2016). GEM emissions from naturally Hg-enriched soils in China have significantly negative δ^{202}Hg ($-4.64‰$ to $-1.10‰$, mean $[\pm 1\sigma] = -2.84 \pm 0.67‰$, $n = 50$) and positive Δ^{199}Hg ($-0.06‰$ to $0.88‰$, mean $[\pm 1\sigma] = 0.27 \pm 0.18‰$, n = 50; Fu et al., 2017). Combined anthropogenic and soil emissions in China yield mean ($\pm 1\sigma$) δ^{202}Hg and Δ^{199}Hg of $-2.04 \pm 0.65‰$ and $0.15 \pm 0.15\%$ (Table S4), respectively, which are comparable to our estimates of GEM emissions in mainland China.

It is challenging to quantify the isotopic signatures of background atmospheric GEM pool in East Asia because all the integrated GEM samples collected here were a mixture of Hg emitted from the sources and background atmospheric pool (Table S1). As shown in Figures 1 and S3, atmospheric GEM at HNI with concentrations lower than the background (e.g., 1.5 ng/m^3) in the Northern Hemisphere were mostly related to air masses from open seas of ECS and Yellow Sea and the free troposphere over Northeast Asia, whereas GEM with concentrations higher than 1.5 ng/m^3 were mostly related to outflow of Hg from mainland China. Therefore, atmospheric GEM with concentrations lower than 1.5 ng/m^3 reflected a minor influence of direct Hg emissions and likely represented the background of atmospheric GEM in East Asia. At HNI, 16.4% of the

total 7264 observations (5-min mean measured by Tekran system) had GEM concentrations less than background of 1.50 ng/m^3. The average concentration of these background GEM samples was 1.36 ± 0.10 ng/m^3. This value is well within the range (1.20–1.5 ng/m^3) estimated by modeling studies (Pan et al., 2006; Strode et al., 2008). Hence, the δ^{202}Hg and Δ^{199}Hg signatures of the regional background atmospheric GEM pool should be at 0.58‰ and −0.26‰, respectively. The Δ^{199}Hg signature of the background atmospheric GEM pool in East Asia is comparable to the background observations in North America and Europe (mean [±1σ] = −0.21 ± 0.04‰), while the δ^{202}Hg signature of GEM was relatively lower than the background observations in North America and Europe (mean (±1σ) = 0.84 ± 0.22‰; Demers et al., 2013, 2015; Enrico et al., 2016; Fu, Maruszczak, Wang, et al., 2016; Obrist et al., 2017).

4. Conclusion

In this study, atmospheric GEM, PBM, and GOM concentrations and GEM isotopic composition were measured at HNI in the MBL of ECS, which regularly received Hg-polluted plumes from mainland China and clean air masses from open seas and free troposphere in East Asia. The data set provided an evidence that outflow of Hg from mainland China strongly influenced the concentrations and isotopic compositions of atmospheric GEM in the MBL of Asia marginal seas. On the basis of the observations, we suggest that GEM emissions in mainland China are characterized by highly negative δ^{202}Hg (−1.79 ± 0.24‰, 1σ) and near-zero Δ^{199}Hg (0.02 ± 0.04‰, 1σ) signatures, and the background regional atmospheric GEM pool was characterized by moderate positive δ^{202}Hg (0.58‰) and negative Δ^{199}Hg (−0.26‰), providing an useful clue to track the impact of Chinese Hg emissions on regional and global atmospheric GEM budget. Highly negative δ^{202}Hg$_{GEM}$ signature of Chinese Hg emissions suggested a larger contribution of GEM emissions from coal combustion lacking conventional APCDs, cement and mercury production, biomass burning, and soil emissions to the total GEM emissions in China. We caution that due to the poor understanding of isotopic compositions of GEM emitted from various emission sources and fractionation processes of Hg isotopes during atmospheric transformations, use of isotopic signatures for atmospheric Hg source apportionment still has large uncertainties. Therefore, more research regarding the isotopic compositions of Hg emitted from various anthropogenic and natural sources as well as the transformation induced fractionation of atmospheric Hg isotopes is needed.

References

Bergquist, B. A., & Blum, J. D. (2007). Mass-dependent and -independent fractionation of Hg isotopes by photoreduction in aquatic systems. *Science*, *318*(5849), 417–420. https://doi.org/10.1126/science.1148050

Biswas, A., Blum, J. D., Bergquist, B. A., Keeler, G. J., & Xie, Z. Q. (2008). Natural mercury isotope variation in coal deposits and organic soils. *Environmental Science & Technology*, *42*(22), 8303–8309. https://doi.org/10.1021/Es801444b

Blum, J. D., & Bergquist, B. A. (2007). Reporting of variations in the natural isotopic composition of mercury. *Analytical and Bioanalytical Chemistry*, *388*(2), 353–359. https://doi.org/10.1007/s00216-007-1236-9

Blum, J. D., Sherman, L. S., & Johnson, M. W. (2014). Mercury isotopes in Earth and environmental sciences. *Annual Review of Earth and Planetary Sciences*, *42*(1), 249–269. https://doi.org/10.1146/annurev-earth-050212-124107

Chand, D., Jaffe, D., Prestbo, E., Swartzendruber, P. C., Hafner, W., Weiss-Penzias, P., et al. (2008). Reactive and particulate mercury in the Asian marine boundary layer. *Atmospheric Environment*, *42*(34), 7988–7996. https://doi.org/10.1016/j.atmosenv.2008.06.048

Chen, H. S., Wang, Z. F., Li, J., Tang, X., Ge, B. Z., Wu, X. L., et al. (2015). GNAQPMS-Hg v1.0, a global nested atmospheric mercury transport model: Model description, evaluation and application to trans-boundary transport of Chinese anthropogenic emissions. *Geoscientific Model Development*, *8*(9), 2857–2876. https://doi.org/10.5194/gmd-8-2857-2015

Chen, J. B., Hintelmann, H., Feng, X. B., & Dimock, B. (2012). Unusual fractionation of both odd and even mercury isotopes in precipitation from Peterborough, ON, Canada. *Geochim Cosmochim Ac*, *90*, 33–46. https://doi.org/10.1016/j.gca.2012.05.005

Chen, L., Wang, H. H., Liu, J. F., Tong, Y. D., Ou, L. B., Zhang, W., et al. (2014). Intercontinental transport and deposition patterns of atmospheric mercury from anthropogenic emissions. *Atmospheric Chemistry and Physics*, *14*(18), 10,163–10,176. https://doi.org/10.5194/acp-14-10163-2014

Cheng, I., Xu, X., & Zhang, L. (2015). Overview of receptor-based source apportionment studies for speciated atmospheric mercury. *Atmospheric Chemistry and Physics*, *15*(14), 7877–7895. https://doi.org/10.5194/acp-15-7877-2015

Demers, J. D., Blum, J. D., & Zak, D. R. (2013). Mercury isotopes in a forested ecosystem: Implications for air-surface exchange dynamics and the global mercury cycle. *Global Biogeochemical Cycles*, *27*, 222–238. https://doi.org/10.1002/Gbc.20021

Demers, J. D., Sherman, L. S., Blum, J. D., Marsik, F. J., & Dvonch, J. T. (2015). Coupling atmospheric mercury isotope ratios and meteorology to identify sources of mercury impacting a coastal urban-industrial region near Pensacola, Florida, USA. *Global Biogeochemical Cycles*, *29*, 1689–1705. https://doi.org/10.1002/2015GB005146

Engstrom, A., & Magnusson, L. (2009). Estimating trajectory uncertainties due to flow dependent errors in the atmospheric analysis. *Atmospheric Chemistry and Physics*, *9*(22), 8857–8867. https://doi.org/10.5194/acp-9-8857-2009

Enrico, M., Le Roux, G., Maruszczak, N., Heimburger, L. E., Claustres, A., Fu, X. W., et al. (2016). Atmospheric mercury transfer to peat bogs dominated by gaseous elemental mercury dry deposition. *Environmental Science & Technology*, *50*(5), 2405–2412. https://doi.org/10.1021/acs.est.5b06058

Estrade, N., Carignan, J., Sonke, J. E., & Donard, O. F. X. (2009). Mercury isotope fractionation during liquid-vapor evaporation experiments. *Geochimica et Cosmochimica Acta*, *73*(10), 2693–2711. https://doi.org/10.1016/j.gca.2009.01.024

Estrade, N., Carignan, J., Sonke, J. E., & Donard, O. F. X. (2010). Measuring Hg isotopes in bio-geo-environmental reference materials. *Geostandards and Geoanalytical Research*, *34*(1), 79–93. https://doi.org/10.1111/j.1751-908X.2009.00040.x

Friedli, H. R., Radke, L. F., & Lu, J. Y. (2001). Mercury in smoke from biomass fires. *Geophysical Research Letters*, *28*, 3223–3226. https://doi.org/10.1029/2000GL012704

Fu, X., Maruszczak, N., Wang, X., Gheusi, F., & Sonke, J. E. (2016). Isotopic composition of gaseous elemental mercury in the free troposphere of the Pic du Midi Observatory, France. *Environmental Science & Technology*, *50*(11), 5641–5650. https://doi.org/10.1021/acs.est.6b00033

Fu, X., Zhu, W., Zhang, H., Sommar, J., Yu, B., Yang, X., et al. (2016). Depletion of atmospheric gaseous elemental mercury by plant uptake at Mt. Changbai, Northeast China. *Atmospheric Chemistry and Physics*, *16*(20), 12,861–12,873. https://doi.org/10.5194/acp-16-12861-2016

Fu, X. W., Heimburger, L. E., & Sonke, J. E. (2014). Collection of atmospheric gaseous mercury for stable isotope analysis using iodine- and chlorine-impregnated activated carbon traps. *Journal of Analytical Atomic Spectrometry*, *29*(5), 841–852. https://doi.org/10.1039/C3ja50356a

Fu, X. W., Maruszczak, N., Heimburger, L. E., Sauvage, B., Gheusi, F., Prestbo, E. M., & Sonke, J. E. (2016). Atmospheric mercury speciation dynamics at the high-altitude Pic du Midi Observatory, southern France. *Atmospheric Chemistry and Physics*, *16*(9), 5623–5639. https://doi.org/10.5194/acp-16-5623-2016

Fu, X. W., Tan, Q. Y., & Feng, X. B. (2017). Mercury isotope fractionation during thermal- and photo-induced emission of Hg0 from soil. Paper presented at Proceedings of 13th International Conference on Mercury as a Global Pollutant, Providence, Rhode Island.

Fu, X. W., Zhang, H., Yu, B., Wang, X., Lin, C. J., & Feng, X. B. (2015). Observations of atmospheric mercury in China: A critical review. *Atmospheric Chemistry and Physics*, *15*(16), 9455–9476. https://doi.org/10.5194/acp-15-9455-2015

Gratz, L. E., Keeler, G. J., Blum, J. D., & Sherman, L. S. (2010). Isotopic composition and fractionation of mercury in Great Lakes precipitation and ambient air. *Environmental Science & Technology*, *44*(20), 7764–7770. https://doi.org/10.1021/Es100383w

Gustin, M. S., Amos, H. M., Huang, J., Miller, M. B., & Heidecorn, K. (2015). Measuring and modeling mercury in the atmosphere: A critical review. *Atmospheric Chemistry and Physics*, *15*(10), 5697–5713. https://doi.org/10.5194/acp-15-5697-2015

Kritee, K., Blum, J. D., & Barkay, T. (2008). Mercury stable isotope fractionation during reduction of Hg (II) by different microbial pathways. *Environmental Science & Technology*, *42*(24), 9171–9177. https://doi.org/10.1021/Es801591k

Lamborg, C. H., Hammerschmidt, C. R., Bowman, K. L., Swarr, G. J., Munson, K. M., Ohnemus, D. C., et al. (2014). A global ocean inventory of anthropogenic mercury based on water column measurements. *Nature*, *512*(7512), 65–68. https://doi.org/10.1038/Nature13563

Landis, M. S., Ryan, J. V., ter Schure, A. F. H., & Laudal, D. (2014). Behavior of mercury emissions from a commercial coal-fired power plant: The relationship between stack speciation and near-field plume measurements. *Environmental Science & Technology*, *48*(22), 13,540–13,548. https://doi.org/10.1021/es500783t

Laurier, F., & Mason, R. (2007). Mercury concentration and speciation in the coastal and open ocean boundary layer. *Journal of Geophysical Research*, *112*, D06302. https://doi.org/10.1029/2006JD007320

Laurier, F. J. G., Mason, R. P., Whalin, L., & Kato, S. (2003). Reactive gaseous mercury formation in the North Pacific Ocean's marine boundary layer: A potential role of halogen chemistry. *Journal of Geophysical Research*, *108*(D17), 4529. https://doi.org/10.1029/2003JD003625

Lefticariu, L., Blum, J. D., & Gleason, J. D. (2011). Mercury isotopic evidence for multiple mercury sources in coal from the Illinois Basin. *Environmental Science & Technology*, *45*(4), 1724–1729. https://doi.org/10.1021/Es102875n

Lin, C. J., Pan, L., Streets, D. G., Shetty, S. K., Jang, C., Feng, X., et al. (2010). Estimating mercury emission outflow from East Asia using CMAQ-Hg. *Atmospheric Chemistry and Physics*, *10*(4), 1853–1864. https://doi.org/10.5194/acp-10-1853-2010

Lindberg, S., Bullock, R., Ebinghaus, R., Engstrom, D., Feng, X. B., Fitzgerald, W., et al. (2007). A synthesis of progress and uncertainties in attributing the sources of mercury in deposition. *Ambio*, *36*(1), 19–33. https://doi.org/10.1579/0044-7447(2007)36[19:ASOPAU]2.0.CO;2

Malcolm, E. G., Keeler, G. J., & Landis, M. S. (2003). The effects of the coastal environment on the atmospheric mercury cycle. *Journal of Geophysical Research*, *108*(D12), 4357. https://doi.org/10.1029/2002JD003084

Mao, H. T., Cheng, I., & Zhang, L. M. (2016). Current understanding of the driving mechanisms for spatiotemporal variations of atmospheric speciated mercury: A review. *Atmospheric Chemistry and Physics*, *16*(20), 12,897–12,924. https://doi.org/10.5194/acp-16-12897-2016

Muntean, M., Janssens-Maenhout, G., Song, S. J., Selin, N. E., Olivier, J. G. J., Guizzardi, D., et al. (2014). Trend analysis from 1970 to 2008 and model evaluation of EDGARv4 global gridded anthropogenic mercury emissions. *Science of the Total Environment*, *494*, 337–350. https://doi.org/10.1016/j.scitotenv.2014.06.014

Obrist, D., Agnan, Y., Jiskra, M., Olson, C. L., Colegrove, D. P., Hueber, J., et al. (2017). Tundra uptake of atmospheric elemental mercury drives Arctic mercury pollution. *Nature*, *547*(7662), 201–204. https://doi.org/10.1038/nature22997

Pacyna, E. G., Pacyna, J. M., Sundseth, K., Munthe, J., Kindbom, K., Wilson, S., et al. (2010). Global emission of mercury to the atmosphere from anthropogenic sources in 2005 and projections to 2020. *Atmospheric Environment*, *44*(20), 2487–2499. https://doi.org/10.1016/j.atmosenv.2009.06.009

Pan, L., Lin, C. J., Carmichael, G. R., Streets, D. G., Tang, Y. H., Woo, J. H., et al. (2010). Study of atmospheric mercury budget in East Asia using STEM-Hg modeling system. *Science of the Total Environment*, *408*(16), 3277–3291. https://doi.org/10.1016/j.scitotenv.2010.04.039

Pan, L., Woo, J. H., Carmichael, G. R., Tang, Y. H., Friedli, H. R., & Radke, L. F. (2006). Regional distribution and emissions of mercury in East Asia: A modeling analysis of Asian Pacific Regional Aerosol Characterization Experiment (ACE-Asia) observations. *Journal of Geophysical Research*, *111*, D07109. https://doi.org/10.1029/2005JD006381

Pirrone, N., Cinnirella, S., Feng, X., Finkelman, R. B., Friedli, H. R., Leaner, J., et al. (2010). Global mercury emissions to the atmosphere from anthropogenic and natural sources. *Atmospheric Chemistry and Physics*, *10*(13), 5951–5964. https://doi.org/10.5194/acp-10-5951-2010

Rodriguez-Gonzalez, P., Epov, V. N., Bridou, R., Tessier, E., Guyoneaud, R., Monperrus, M., & Amouroux, D. (2009). Species-specific stable isotope fractionation of mercury during Hg (II) methylation by an anaerobic bacteria (Desulfobulbus propionicus) under dark conditions. *Environmental Science & Technology*, *43*(24), 9183–9188. https://doi.org/10.1021/es902206j

Rolison, J. M., Landing, W. M., Luke, W., Cohen, M., & Salters, V. J. M. (2013). Isotopic composition of species-specific atmospheric Hg in a coastal environment. *Chemical Geology*, *336*, 37–49. https://doi.org/10.1016/j.chemgeo.2012.10.007

Selin, N. E., Jacob, D. J., Park, R. J., Yantosca, R. M., Strode, S., Jaegle, L., & Jaffe, D. (2007). Chemical cycling and deposition of atmospheric mercury: Global constraints from observations. *Journal of Geophysical Research*, *112*, D02308. https://doi.org/10.1029/2006JD007450

Sherman, L. S., Blum, J. D., Johnson, K. P., Keeler, G. J., Barres, J. A., & Douglas, T. A. (2010). Mass-independent fractionation of mercury isotopes in Arctic snow driven by sunlight. *Nature Geoscience*, *3*(3), 173–177. https://doi.org/10.1038/Ngeo758

Slemr, F., Angot, H., Dommergue, A., Magand, O., Barret, M., Weigelt, A., et al. (2015). Comparison of mercury concentrations measured at several sites in the Southern Hemisphere. *Atmospheric Chemistry and Physics*, *15*(6), 3125–3133. https://doi.org/10.5194/acp-15-3125-2015

Smith, C. N., Kesler, S. E., Blum, J. D., & Rytuba, J. J. (2008). Isotope geochemistry of mercury in source rocks, mineral deposits and spring deposits of the California Coast Ranges, USA. *Earth and Planetary Science Letters*, *269*(3–4), 398–406

Soerensen, A. L., Sunderland, E. M., Holmes, C. D., Jacob, D. J., Yantosca, R. M., Skov, H., et al. (2010). An improved global model for air-sea exchange of mercury: High concentrations over the North Atlantic. *Environmental Science & Technology*, *44*(22), 8574–8580. https://doi.org/10.1021/Es102032g

Sonke, J. E., & Blum, J. D. (2013). Advances in mercury stable isotope biogeochemistry preface. *Chemical Geology*, *336*, 1–4. https://doi.org/10.1016/j.chemgeo.2012.10.035

Sonke, J. E., Schafer, J., Chmeleff, J., Audry, S., Blanc, G., & Dupre, B. (2010). Sedimentary mercury stable isotope records of atmospheric and riverine pollution from two major European heavy metal refineries. *Chemical Geology*, *279*(3–4), 90–100. https://doi.org/10.1016/j.chemgeo.2010.09.017

Sprovieri, F., Pirrone, N., Bencardino, M., D'Amore, F., Carbone, S., Cinnirella, V., et al. (2016). Atmospheric mercury concentrations observed at ground-based monitoring sites globally distributed in the framework of the GMOS network. *Atmospheric Chemistry and Physics*, *16*(18), 11,915–11,935. https://doi.org/10.5194/acp-16-11915-2016

Sprovieri, F., Pirrone, N., Gardfeldt, K., & Sommar, J. (2003). Mercury speciation in the marine boundary layer along a 6000 km cruise path around the Mediterranean Sea. *Atmospheric Environment*, *37*, S63–S71. https://doi.org/10.1016/S1352-2310(03)00237-1

Strode, S. A., Jaegle, L., Jaffe, D. A., Swartzendruber, P. C., Selin, N. E., Holmes, C., & Yantosca, R. M. (2008). Trans-Pacific transport of mercury. *Journal of Geophysical Research*, *113*, D15305. https://doi.org/10.1029/2007JD009428

Strode, S. A., Jaegle, L., Selin, N. E., Jacob, D. J., Park, R. J., Yantosca, R. M., et al. (2007). Air-sea exchange in the global mercury cycle. *Global Biogeochemical Cycles*, *21*, GB1017. https://doi.org/10.1029/2006GB002766

Sun, R. Y., Enrico, M., Heimburger, L. E., Scott, C., & Sonke, J. E. (2013). A double-stage tube furnace-acid-trapping protocol for the preconcentration of mercury from solid samples for isotopic analysis. *Analytical and Bioanalytical Chemistry*, *405*(21), 6771–6781. https://doi.org/10.1007/s00216-013-7152-2

Sun, R. Y., Heimburger, L. E., Sonke, J. E., Liu, G. J., Amouroux, D., & Berail, S. (2013). Mercury stable isotope fractionation in six utility boilers of two large coal-fired power plants. *Chemical Geology*, *336*, 103–111. https://doi.org/10.1016/j.chemgeo.2012.10.055

Sun, R. Y., Sonke, J. E., Heimburger, L. E., Belkin, H. E., Liu, G. J., Shome, D., et al. (2014). Mercury stable isotope signatures of world coal deposits and historical coal combustion emissions. *Environmental Science & Technology*, *48*(13), 7660–7668. https://doi.org/10.1021/Es501208a

Sun, R. Y., Streets, D. G., Horowitz, H. M., Amos, H. M., Liu, G. J., Perrot, V., et al. (2016). Historical (1850–2010) mercury stable isotope inventory from anthropogenic sources to the atmosphere. *Elementa: Science of the Anthropocene*, *4*(91), https://doi.org/10.12952/journal.elementa.000091

Swartzendruber, P. C., Jaffe, D. A., Prestbo, E. M., Weiss-Penzias, P., Selin, N. E., Park, R., et al. (2006). Observations of reactive gaseous mercury in the free troposphere at the Mount Bachelor Observatory. *Journal of Geophysical Research*, *111*, D24301. https://doi.org/10.1029/2006JD007415

Tang, S., Feng, C., Feng, X., Zhu, J., Sun, R., Fan, H., et al. (2017). Stable isotope composition of mercury forms in flue gases from a typical coal-fired power plant, Inner Mongolia, northern China. *Journal of Hazardous Materials*, *328*, 90–97. https://doi.org/10.1016/j.jhazmat.2017.01.014

Thibodeau, A. M., Ritterbush, K., Yager, J. A., West, A. J., Ibarra, Y., Bottjer, D. J., et al. (2016). Mercury anomalies and the timing of biotic recovery following the end-Triassic mass extinction. *Nature Communications*, *7*. https://doi.org/10.1038/ncomms11147

Wang, F., Saiz-Lopez, A., Mahajan, A. S., Martin, J. C. G., Armstrong, D., Lemes, M., et al. (2014). Enhanced production of oxidised mercury over the tropical Pacific Ocean: A key missing oxidation pathway. *Atmospheric Chemistry and Physics*, *14*(3), 1323–1335. https://doi.org/10.5194/acp-14-1323-2014

Wang, X., Lin, C. J., Yuan, W., Sommar, J., Zhu, W., & Feng, X. B. (2016). Emission-dominated gas exchange of elemental mercury vapor over natural surfaces in China. *Atmospheric Chemistry and Physics*, *16*(17), 11,125–11,143. https://doi.org/10.5194/acp-16-11125-2016

Wang, Y. Q., Zhang, X. Y., & Draxler, R. R. (2009). TrajStat: GIS-based software that uses various trajectory statistical analysis methods to identify potential sources from long-term air pollution measurement data. *Environmental Modelling and Software*, *24*(8), 938–939. https://doi.org/10.1016/j.envsoft.2009.01.004

Wiederhold, J. G., Cramer, C. J., Daniel, K., Infante, I., Bourdon, B., & Kretzschmar, R. (2009). Equilibrium mercury isotope fractionation between dissolved Hg (II) species and thiol-bound Hg. *Geochimica et Cosmochimica Acta*, *73*(13), A1,438–A1,438.

Wright, L. P., Zhang, L. M., & Marsik, F. J. (2016). Overview of mercury dry deposition, litterfall, and throughfall studies. *Atmospheric Chemistry and Physics*, *16*(21), 13,399–13,416. https://doi.org/10.5194/acp-16-13399-2016

Wu, Q. R., Wang, S. X., Li, G. L., Liang, S., Lin, C. J., Wang, Y. F., et al. (2016). Temporal trend and spatial distribution of speciated atmospheric mercury emissions in China during 1978–2014. *Environmental Science & Technology*, *50*(24), 13,428–13,435. https://doi.org/10.1021/acs.est.6b04308

Xu, H., Sonke, J. E., Guinot, B., Fu, X., Sun, R., Lanzanova, A., et al. (2017). Seasonal and annual variations in atmospheric Hg and Pb isotopes in Xi'an, China. *Environmental Science & Technology*, *51*(7), 3759–3766. https://doi.org/10.1021/acs.est.6b06145

Yin, R. S., Feng, X. B., Chen, B. W., Zhang, J. J., Wang, W. X., & Li, X. D. (2015). Identifying the sources and processes of mercury in subtropical estuarine and ocean sediments using Hg isotopic composition. *Environmental Science & Technology*, *49*(3), 1347–1355. https://doi.org/10.1021/es504070y

Yin, R. S., Feng, X. B., & Chen, J. B. (2014). Mercury stable isotopic compositions in coals from major coal producing fields in China and their geochemical and environmental implications. *Environmental Science & Technology*, *48*(10), 5565–5574. https://doi.org/10.1021/Es500322n

Yin, R. S., Feng, X. B., Foucher, D., Shi, W. F., Zhao, Z. Q., & Wang, J. (2010). High precision determination of mercury isotope ratios using online mercury vapor generation system coupled with multi-collector inductively coupled plasma-mass spectrometry. *Chinese*, *Journal of Analytical Chemistry*, *38*(7), 929–934. https://doi.org/10.3724/Sp.J.1096.2010.00929

Yin, R. S., Feng, X. B., Hurley, J. P., Krabbenhoft, D., Lepak, R. F., Hu, R. Z., et al. (2016). Mercury isotopes as proxies to identify sources and environmental impacts of mercury in sphalerites. *Scientific Reports-Uk*, (6), 18686. https://doi.org/10.1038/srep18686

Yin, R. S., Feng, X. B., Wang, J. X., Li, P., Liu, J. L., Zhang, Y., et al. (2013). Mercury speciation and mercury isotope fractionation during ore roasting process and their implication to source identification of downstream sediment in the Wanshan mercury mining area, SW China. *Chemical Geology*, *336*, 72–79. https://doi.org/10.1016/j.chemgeo.2012.04.030

Yu, B., Fu, X., Yin, R., Zhang, H., Wang, X., Lin, C.-J., et al. (2016). Isotopic composition of atmospheric mercury in China: New evidence for sources and transformation processes in air and in vegetation. *Environmental Science & Technology*, *50*(17), 9262–9269. https://doi.org/10.1021/acs.est.6b01782

Zhang, L., Wang, S. X., Wang, L., Wu, Y., Duan, L., Wu, Q. R., et al. (2015). Updated emission inventories for speciated atmospheric mercury from anthropogenic sources in China. *Environmental Science & Technology*, *49*(5), 3185–3194. https://doi.org/10.1021/Es504840m

Zhang, L. M., Wu, Z. Y., Cheng, I., Wright, L. P., Olson, M. L., Gay, D. A., et al. (2016). The estimated six-year mercury dry deposition across North America. *Environmental Science & Technology*, *50*(23), 12,864–12,873. https://doi.org/10.1021/acs.est.6b04276

Zheng, W., Foucher, D., & Hintelmann, H. (2007). Mercury isotope fractionation during volatilization of Hg(0) from solution into the gas phase. *Journal of Analytical Atomic Spectrometry*, *22*(9), 1097–1104. https://doi.org/10.1039/B705677j

Zheng, W., & Hintelmann, H. (2009). Mercury isotope fractionation during photoreduction in natural water is controlled by its Hg/DOC ratio. *Geochimica et Cosmochimica Acta*, *73*(22), 6704–6715. https://doi.org/10.1016/j.gca.2009.08.016

Zheng, W., Obrist, D., Weis, D., & Bergquist, B. A. (2016). Mercury isotope compositions across North American forests. *Global Biogeochemical Cycles*, *30*, 1475–1492. https://doi.org/10.1002/2015GB005323

Zhu, W., Lin, C. J., Wang, X., Sommar, J., Fu, X. W., & Feng, X. B. (2016). Global observations and modeling of atmosphere-surface exchange of elemental mercury: A critical review. *Atmospheric Chemistry and Physics*, *16*(7), 4451–4480. https://doi.org/10.5194/acp-16-4451-2016